

Research Paper

## Green Fabrication of NiO–SnO<sub>2</sub> Nanocomposites Using Grape Extract and Their Application in Cadmium Removal from Water

Seyyed Jalal Roudbaraki\*

*Department of Chemistry, La.C., Islamic Azad University, Lahijan, Iran.*

### ARTICLE INFO

#### Article history:

Received 22 January 2026

Revised: 16 February 2026

Accepted 25 February 2026

Available online 23 October 2024

#### Keywords:

*NiO–SnO<sub>2</sub> nanocomposite*

*green synthesis*

*cadmium adsorption*

*grape extract*

*wastewater treatment*

*nickel oxide*

*tin oxide*

### ABSTRACT

In this work, an environmentally benign approach was developed for the preparation of NiO–SnO<sub>2</sub> nanocomposites employing grape extract as a natural reducing and stabilizing medium. The bio-assisted synthesis route eliminates the need for hazardous chemicals and promotes sustainable material production. The obtained nanocomposites were comprehensively characterized using X-ray diffraction (XRD) to determine crystalline phases, field-emission scanning electron microscopy (FESEM) to investigate surface morphology, dynamic light scattering (DLS) for particle size distribution, and Brunauer–Emmett–Teller (BET) analysis to evaluate specific surface area and porosity. The adsorption capability of the synthesized material was examined for the removal of Cd<sup>2+</sup> ions from aqueous solutions at room temperature. Experimental findings demonstrated that the grape-extract-derived nanocomposite exhibited superior adsorption efficiency compared to conventionally prepared counterparts. Furthermore, adsorption kinetics and thermodynamic parameters were evaluated to gain deeper insight into the interaction mechanism between cadmium ions and the nanocomposite surface. The results confirm the potential of this green-synthesized NiO–SnO<sub>2</sub> system as an effective and sustainable adsorbent for heavy metal remediation in water treatment applications.

**Citation:** Roudbaraki, S.J. (2024). Green Fabrication of NiO–SnO<sub>2</sub> Nanocomposites Using Grape Extract and Their Application in Cadmium Removal from Water, Journal of Advanced Materials and Processing, 12 (48), 3-12. Doi: 10.71670/jmatpro.2024.1231798

#### Copyrights:

Copyright for this article is retained by the author (s), with publication rights granted to Journal of Advanced Materials and Processing. This is an open – access article distributed under the terms of the Creative Commons Attribution License (<http://creativecommons.org/licenses/by/4.0>), which permits unrestricted use, distribution and reproduction in any medium, provided the original work is properly cited.



\* Corresponding Author:

E-Mail: roudbarakiseyedjalal@gmail.com

## 1. Introduction

In recent years, tin (IV) oxide ( $\text{SnO}_2$ ) nanoparticles have attracted considerable scientific and technological interest due to their versatile functionality in environmental and industrial fields. Their applications extend to manufacturing processes, analytical systems, gas monitoring technologies, and pollution mitigation platforms. The widespread attention devoted to  $\text{SnO}_2$  is primarily associated with its remarkable physicochemical attributes, which have established it as one of the most intensively studied metal oxides. This material exhibits high chemical stability, appreciable electrical conductivity, and effective catalytic activity. Moreover, the presence of a wide band gap provides advantageous optical and electronic properties, supporting its integration into gas sensors, transparent conducting coatings, and related optoelectronic devices [1–8].

The performance of  $\text{SnO}_2$  can be strategically modified through compositional engineering, particularly by coupling it with other metal oxides to form composite or heterostructured architectures. Such structural integration frequently produces cooperative or synergistic interactions that enhance overall functionality beyond that of the individual constituents. For example,  $\text{SnO}/\text{SnO}_2$  composite thin films have shown markedly improved responsiveness toward dichloromethane compared with single-component  $\text{SnO}$  or  $\text{SnO}_2$  layers [9].  $\text{Al}_2\text{O}_3\text{-SnO}_2$  nanocomposites have demonstrated elevated photocatalytic efficiency in the degradation of methyl orange [10]. Likewise,  $\text{SnO}_2/\alpha\text{-Fe}_2\text{O}_3$  heteronanostructures have exhibited superior sensing characteristics for dimethyl disulfide when compared with hollow  $\text{SnO}_2$  materials [11]. Composite systems based on  $\text{SnO}_2\text{-TiO}_2$  have also revealed enhanced hydrogen detection capability [12]. In addition,  $\text{ZnO}/\text{SnO}_2$  nanocomposites possess broader band gap energies relative to their individual oxide phases, enabling applications in photocatalysis, optoelectronics, gas sensing, and solar energy conversion [13]. Similarly,  $\text{NiO-SnO}_2$  heterojunction configurations have been reported to significantly improve nitrogen dioxide sensing performance at ambient conditions [14].

Although conventional synthetic methodologies are effective in producing  $\text{SnO}_2$ -based nanomaterials, they often involve hazardous precursors, elevated temperatures, and environmentally detrimental byproducts. These limitations have prompted growing interest in sustainable fabrication techniques. Green and biologically mediated synthesis approaches have therefore emerged as promising alternatives, offering environmentally responsible and economically viable pathways for nanoparticle production. Plant-derived

extracts, in particular, serve as natural reducing and capping agents, facilitating nanoparticle formation while minimizing the use of toxic chemicals and reducing residual contamination [15–20].

To date, environmentally friendly synthesis strategies for  $\text{NiO-SnO}_2$  nanocomposites have received limited attention, underscoring the importance of developing controllable and sustainable preparation routes for such systems. In this work, an eco-conscious synthesis method employing grape extract as a natural reaction medium is introduced for the fabrication of  $\text{NiO-SnO}_2$  nanocomposites. Additionally, the catalytic efficiency of the obtained material is evaluated for cadmium ion removal from contaminated aqueous media, with the objective of demonstrating its applicability in wastewater treatment and environmental remediation.

## 2. Experimental

All chemicals were obtained from Merck and Aldrich and applied as received, without additional purification steps. Reported yields correspond to the isolated materials following purification. Powder X-ray diffraction (XRD) measurements were carried out on a  $\text{D}_8$  Advance Bruker AXS diffractometer employing  $\text{Cu-K}\alpha$  radiation. The morphology of the prepared samples was investigated using a Hitachi S-4160 field emission scanning electron microscope (FESEM). Particle size distribution and surface characteristics were evaluated by dynamic light scattering (DLS) using a Nano ZS (ZEN 3600, red badge) instrument and specific surface area analysis was conducted via the Brunauer–Emmett–Teller (BET) method using a Belsorp Mini II analyzer.

### 2.1. Synthesis of $\text{NiO-SnO}_2$ Nanocomposite

Nickel chloride (20 mmol) and tin(II) chloride (20 mmol) were dissolved in 100 mL of ethanol containing 30 mL of grape extract in a 250 mL beaker to form solution A. In a separate container, 30 mL of aqueous ammonia was mixed with 50 mL of distilled water and supplemented with 10 mL of grape extract to prepare solution B. Solution B was introduced gradually into solution A under continuous and vigorous magnetic stirring. After complete addition, the suspension was further stirred for 1 h to ensure homogeneity and complete precipitation. The obtained solid was separated by filtration, rinsed several times with distilled water to remove residual impurities, and dried in an oven. The dried precursor was subsequently calcined at 500 °C for 3 h to obtain the final  $\text{NiO-SnO}_2$  nanocomposite.

### 2.2. Adsorption Studies

Cadmium sulfate octahydrate ( $\text{CdSO}_4 \cdot 8\text{H}_2\text{O}$ ) served as the cadmium source. Stock and working solutions were prepared by dissolving appropriate quantities of  $\text{CdSO}_4 \cdot 8\text{H}_2\text{O}$  in distilled water. Adsorption performance was evaluated using a batch equilibrium

approach under ambient laboratory conditions. Four initial  $\text{Cd}^{2+}$  concentrations (20, 40, 60, and 80 mg/L) with natural pH values in the range of approximately 5.1–5.8 were prepared. The solution pH was adjusted between 3 and 8 by adding dilute HCl or NaOH solutions as required.

The NiO–SnO<sub>2</sub> adsorbent was introduced into the cadmium solutions and the suspensions were magnetically stirred at room temperature for 100 min. At 20 min intervals, aliquots were withdrawn and analyzed for residual  $\text{Cd}^{2+}$  concentration using atomic absorption spectroscopy (Varian Spectra A 250 Plus). Additional experiments were conducted to investigate the effect of adsorbent dosage (0.025, 0.05, 0.1, and 0.2 g), while maintaining a constant initial  $\text{Cd}^{2+}$  concentration.

The removal efficiency (R), equilibrium adsorption capacity ( $q_e$ ), and adsorption capacity at time t ( $q_t$ ) were calculated according to the following equations:

$$R = \frac{C_0 - C_t}{C_0} * 100 \quad q_t = \frac{(C_0 - C_t) * V}{m} \quad q_e = \frac{(C_0 - C_e) * V}{m}$$

Where  $C_0$  (mg/L) represents the initial  $\text{Cd}^{2+}$  concentration,  $C_t$  (mg/L) is the concentration at time t (min),  $C_e$  (mg/L) denotes the equilibrium concentration, V (L) is the solution volume, and m (g) corresponds to the mass of the adsorbent.

### 3. Results and discussion

#### 3.1. Catalyst Characterization

Initially, pure NiO–SnO<sub>2</sub> nanocrystals were synthesized *via* precipitation from aqueous solutions of NiCl<sub>2</sub> and SnCl<sub>2</sub>. Subsequently, a series of NiO–SnO<sub>2</sub> nanocomposites with varying Ni:Sn molar ratios were prepared through a green co-precipitation approach using grape extract as a bio-reducing and stabilizing medium, thereby avoiding hazardous solvents and chemical additives.

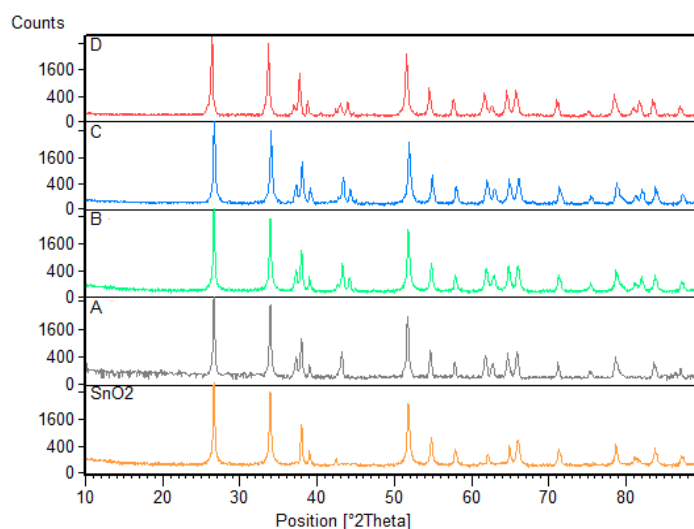


**Fig. 1.** XRD patterns of NiO–SnO<sub>2</sub> (A, without use of grape extract), NiO–SnO<sub>2</sub> (B, 50/50% Ni/Sn ratio of starting materials), NiO–SnO<sub>2</sub> (C, 25/75% Ni/Sn ratio of starting materials), NiO–SnO<sub>2</sub> (D, 10/90% Ni/Sn ratio of starting materials)

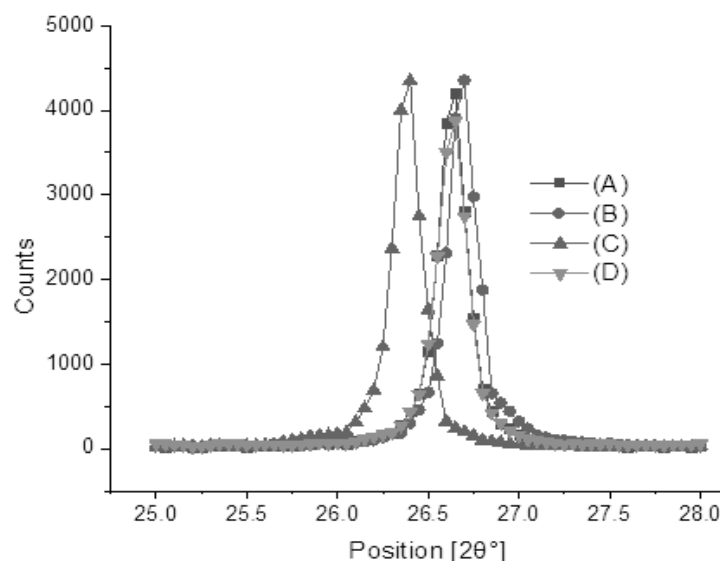


**Fig. 2.** Changes on the peak position of NiO–SnO<sub>2</sub> (A, 50/50% Ni/Sn ratio), NiO–SnO<sub>2</sub> (B, 25/75% Ni/Sn ratio), NiO–SnO<sub>2</sub> (C, 10/90% Ni/Sn ratio), and NiO–SnO<sub>2</sub> (D, without use of grape extract),

The X-ray diffraction (XRD) patterns of the samples calcined at 500°C are presented in Figure 1. The diffraction peaks confirm the coexistence of tetragonal SnO<sub>2</sub> (JCPDS card No. 01-072-1147, space group P42/mnm), with characteristic reflections at 2θ values of 26.6°, 33.9°, 37.9°, 51.8°, 54.8°, 57.8°, 61.9°, 64.8°, 66.0°, and 78.7°, together with rhombohedral NiO (JCPDS card No. 00-044-1159, space group R-3m), exhibiting prominent peaks at 37.2°, 43.3°, 62.8°, 75.4°, and 79.4°. Variations in peak intensity and slight shifts in peak position were observed for nanocomposites with different Ni:Sn ratios (Figure 2), reflecting changes in composition and possible lattice interactions. Notably, the sample synthesized without grape extract displayed weaker diffraction intensities,

suggesting lower crystallinity compared to the bio-assisted samples.

Surface morphology was investigated by FE-SEM (Figure 3). The micrographs reveal that all materials consist of aggregated nanoscale particles with partially amorphous features. In the presence of grape extract, the particles appear more interconnected, likely due to gas evolution during thermal decomposition of organic constituents, which promotes particle adhesion and network formation. In contrast, the sample prepared without extract exhibits less structural integration. Furthermore, decreasing the nickel content leads to reduced particle agglomeration and improved uniformity in morphology.

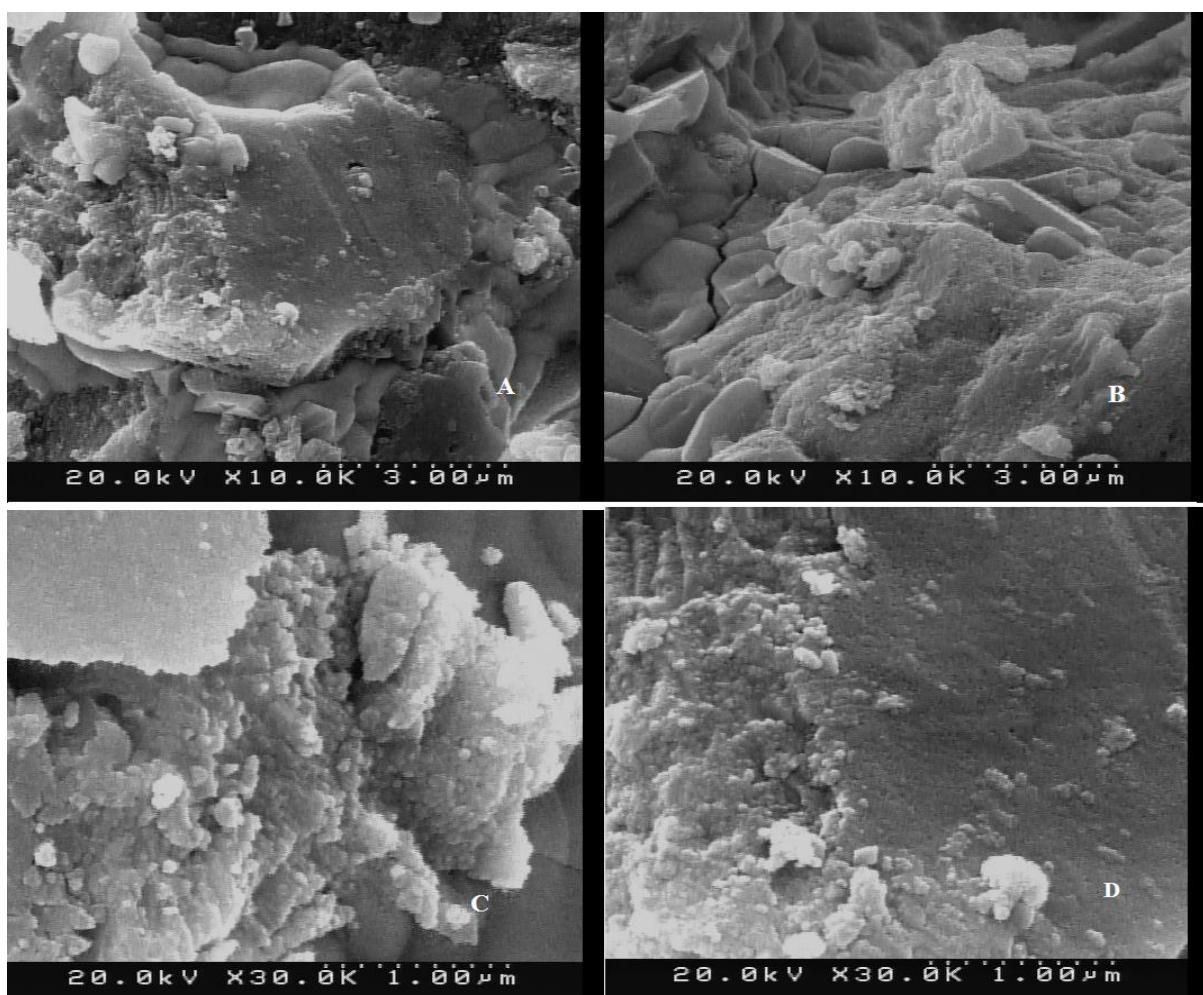


**Fig. 3.** FE-SEM images of NiO-SnO<sub>2</sub> (A, 50/50% Ni/Sn ratio), NiO-SnO<sub>2</sub> (B, 25/75% Ni/Sn ratio), NiO-SnO<sub>2</sub> (C, 10/90% Ni/Sn ratio), and NiO-SnO<sub>2</sub> (D, without use of grape extract)

Particle size distribution was evaluated using DLS analysis. Prior to measurement, each sample was dispersed in ethanol (1 g in 25 mL) and ultrasonicated for 30 min to ensure proper dispersion. The average hydrodynamic diameters were approximately 85 nm (Sample A), 71 nm (Sample B), 60 nm (Sample C),

and 54 nm (Sample D). These findings indicate that the use of grape extract contributes to a narrower and more uniform particle size distribution. Additionally, a decrease in Ni content corresponds to a reduction in mean particle size.

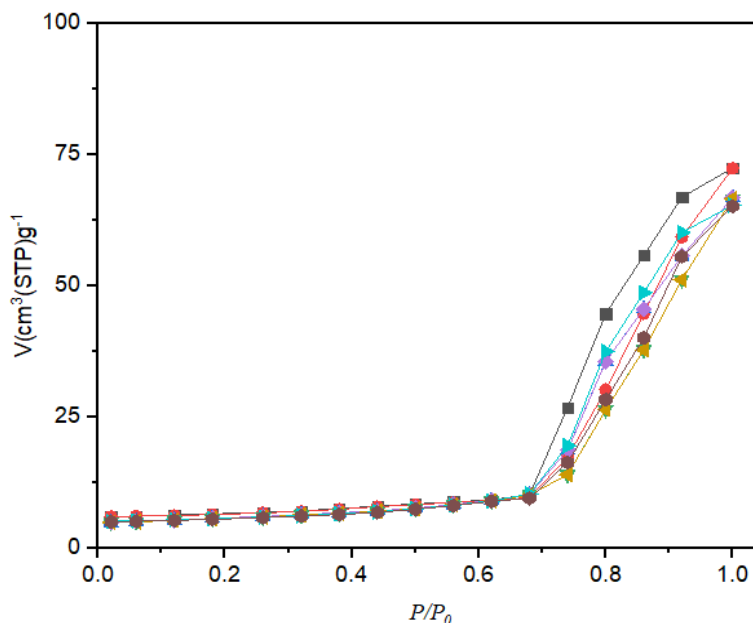


**Fig. 4.** N<sub>2</sub> adsorption- desorption isotherms of NiO-SnO<sub>2</sub> (1, 50/50% Ni/Sn ratio), NiO-SnO<sub>2</sub> (2, 25/75% Ni/Sn ratio), NiO-SnO<sub>2</sub> (3, 10/90% Ni/Sn ratio), and NiO-SnO<sub>2</sub> (4, without use of grape extract)

Nitrogen adsorption–desorption isotherms of the four NiO–SnO<sub>2</sub> nanocomposites are illustrated in Figure 4. According to IUPAC classification, all samples exhibit type IV isotherms accompanied by H3 hysteresis loops, characteristic of mesoporous materials. Among the investigated compositions, the nanocomposite with an equimolar Ni:Sn ratio demonstrates the highest N<sub>2</sub> adsorption capacity. Conversely, the sample synthesized without grape

extract (Sample 4) shows the lowest adsorption performance. Textural parameters, including specific surface area and pore size distribution, were determined using BET and BJH methods, and the results are summarized in Table 1. The data reveal a gradual decline in surface area and pore volume as the NiO content decreases from 50% to 10%, highlighting the influence of composition on the structural properties of the nanocomposites.

**Table 1.** Specific surface area, pore diameter, and pore volume values of NiO-SnO<sub>2</sub> nano-composites

Sample	Specific surface area (m <sup>2</sup> /g)		Pore diameter (nm)
	BET	BJH	BJH
1, 50% Ni	56.98	57.58	7.06
2, 25% Ni	54.42	55.06	5.45
3, 10% Ni	52.97	53.89	4.89
4, without use of grape extract	48.11	49.28	3.15

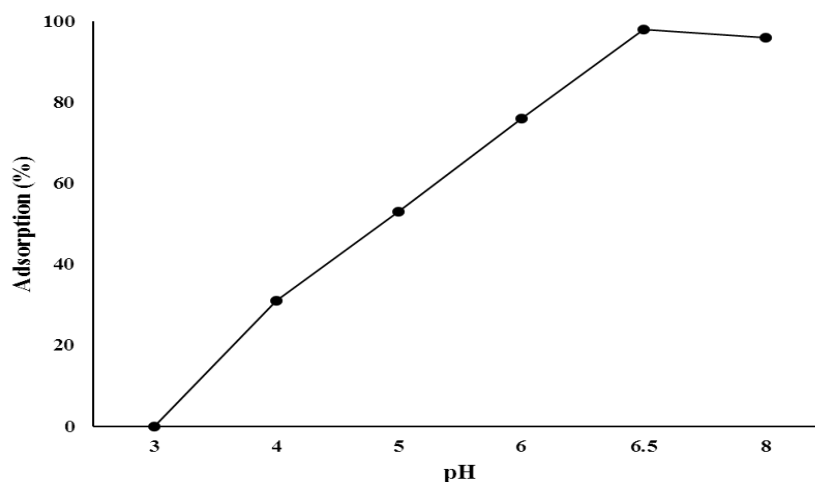


**Fig. 5.** Adsorption of Cd: effect of pH (time: 90min; NiO-SnO<sub>2</sub>: 0.05g; Cd: 40ppm; r.t.)

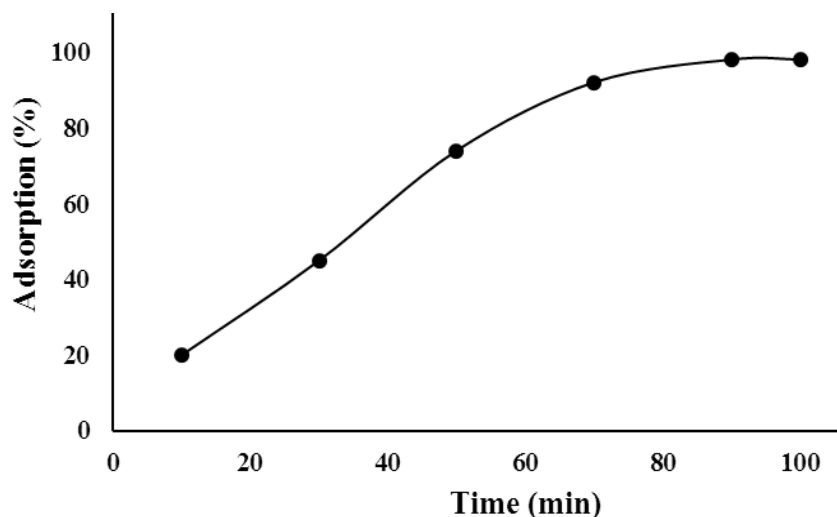


Fig. 6. Adsorption of Cd: effect of contact time (pH: 6.5; NiO-SnO<sub>2</sub>: 0.05g; Cd: 40ppm; r.t.)

### 3.2. Removal of Cd ions

The effect of pH on cadmium adsorption efficiency is shown in Figure 6. As it is shown, the best absorption efficiency occurs in weak acidic media pH = 6.5. As the pH changed from 3 to 8, the amount of cadmium adsorption increased from 0 to 100%. In general, in the adsorption process, the pH of aqueous solution is a very important control parameter because it determines the type of metal ion species and the charge level of the adsorbent. This will affect the reaction between adsorbent and adsorbent material. The effect of pH on the adsorption capacity is related to the chemical state of heavy metal in a solution at different amounts of pH, which can be pure ionic form (Cd<sup>2+</sup>) at acidic media or form hydroxyl-metal (CdOH<sup>+</sup>) in weak basic condition.

Next the effect of contact time on the adsorption capacity was investigated. The results revealed that the adsorption increased rapidly at first 60 min of starting due to high concentration of cadmium ions in the solution. After that, the filling of active sites of nano-composite and low Cd concentration causes the slowly proceeding of adsorption and follows a relatively linear trend (Figure 6).

Comparatively, nano-composite constitute of an equal ratio of Ni and Sn shows better results than those of lower percentage of Ni (Figure 7). In addition nano-composites have higher adsorption capacity than NiO and SnO<sub>2</sub> oxides. Nano-composite prepared without use of grape extract shows lower adsorption capacity than those that prepared in a grape extract media.

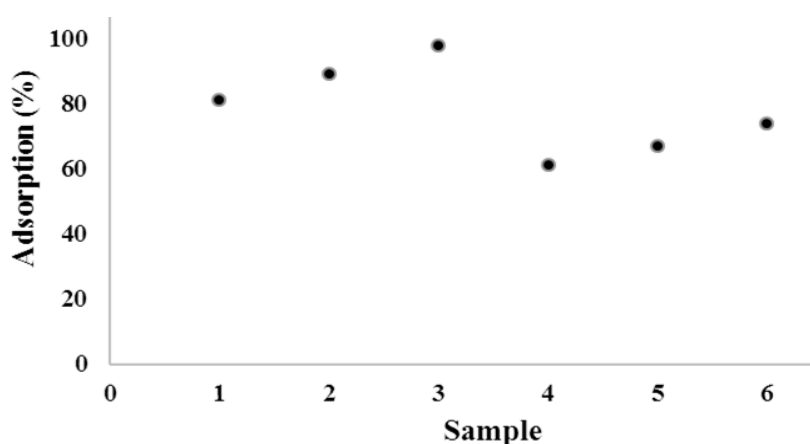


Fig. 7. Adsorption of Cd on the surface of NiO-SnO<sub>2</sub> (1, 10/90% Ni/Sn ratio), NiO-SnO<sub>2</sub> (2, 25/75% Ni/Sn ratio), NiO-SnO<sub>2</sub> (3, 50/50% Ni/Sn ratio), NiO (4), SnO<sub>2</sub> (5), and NiO-SnO<sub>2</sub> (6, without use of grape extract), (time: 90min; cat.: 0.05g; pH: 6.5; Cd: 40ppm; r.t.)

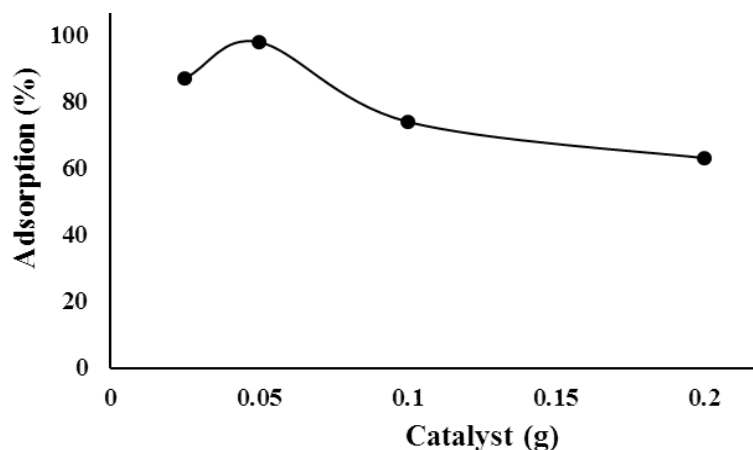


Fig. 8. Adsorption of Cd: effect of catalyst dosage (time: 90min; pH: 6.5; Cd: 40ppm; r.t.)

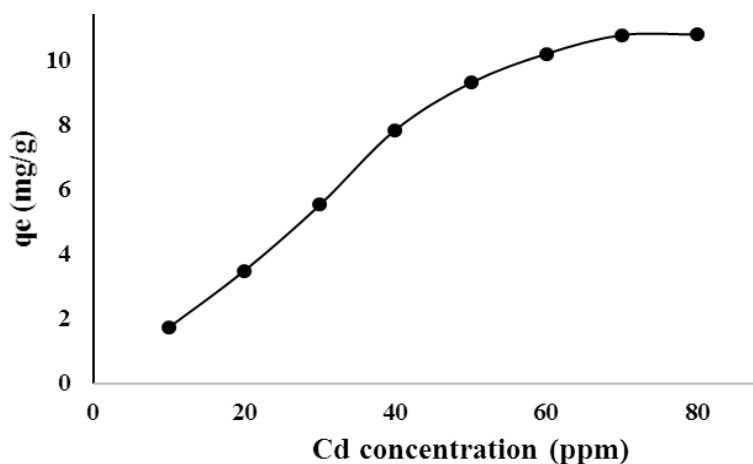


Fig. 9. Adsorption of Cd: effect of initial Cd concentration (time: 90min; cat.: 0.05g; pH: 6.5; r.t.)

Figures 8,9 show the effect of catalyst dosages and the initial concentration of cadmium on the absorption values. It is known that at high Cd concentrations (higher than 40 ppm) the absorption efficiency decreases because of filling of composite active sites. On the other hand, the Cd removal increases up to 0.05 g of the nano-composite dosage and consequently decreased due to agglomeration of composite species and reducing of active sites.

### 3.3. Adsorption kinetics modeling

Generally, absorption depends on the various factors arises from physical and chemical properties of the both adsorbent and absorbent. Thus, absorption kinetics investigation is important for the determination of the adsorption mechanism. In this

study, kinetic behavior and cadmium adsorption mechanism by nano-adsorbent were studied using four kinetic models. Correlation coefficient was used for matching laboratory data with predicted data by kinetic models. Four models including the pseudo-first order, pseudo-second order, Elovich equation, and intra-particle diffusion were evaluated. The equations and extracted data are shown in Table 2. All constant parameters were extracted from fitted linear plots of equations:  $\log(q_e - q_t)$  vs  $t$ ,  $t/q_t$  vs  $t$ ,  $q_t$  vs  $\ln t$ , and  $q_t$  vs  $t^{0.5}$ . The higher correlation coefficient ( $R^2$ ) value of Elovich plot ( $q_t$  vs  $\ln t$ ) indicates that the adsorption mechanism of Cd is chemisorption [21-23]. The  $q_e$  calculated values from pseudo-first order and pseudo-second order equations are different from their experimental data.

**Table 2.** Parameters and correlation coefficient (R<sup>2</sup>) of kinetic models

Model	Linear and nonlinear equations	Parameters
pseudo-first-order	$\log (q_e - q_t) = \log q_e - \frac{kt}{2.303}$ $q_t = q_e(1 - e^{-kt})$	k= 0.048 R <sup>2</sup> = 0.9506; q <sub>e</sub> = 11.65
pseudo-second-order	$\frac{t}{q_t} = \frac{1}{kq_e^2} + \frac{t}{q_e}$ $q_t = \frac{q_e kt}{1 + ktq_e^2}$	k = 0.0025 R <sup>2</sup> = 0.7918; q <sub>e</sub> = 10.89
Elovich equation	$q_t = \frac{\ln(\alpha \cdot \beta)}{\beta} + \frac{\ln t}{\beta}$	β = 0.3242; α = 0.4661 R <sup>2</sup> = 0.9857
Intra-particle diffusion	$q_t = k_i (t)^{0.5} + c$	c = -0.5854; k <sub>i</sub> = 0.9309 R <sup>2</sup> = 0.9727

k is the rate constant (min<sup>-1</sup>), t is the contact time (min), β, α are Elovich constants; k<sub>i</sub> (mg g<sup>-1</sup> min<sup>-1/2</sup>) is the intra-particle diffusion rate constant and c (mg g<sup>-1</sup>) is a constant proportional to the thickness of the boundary layer [21-23].

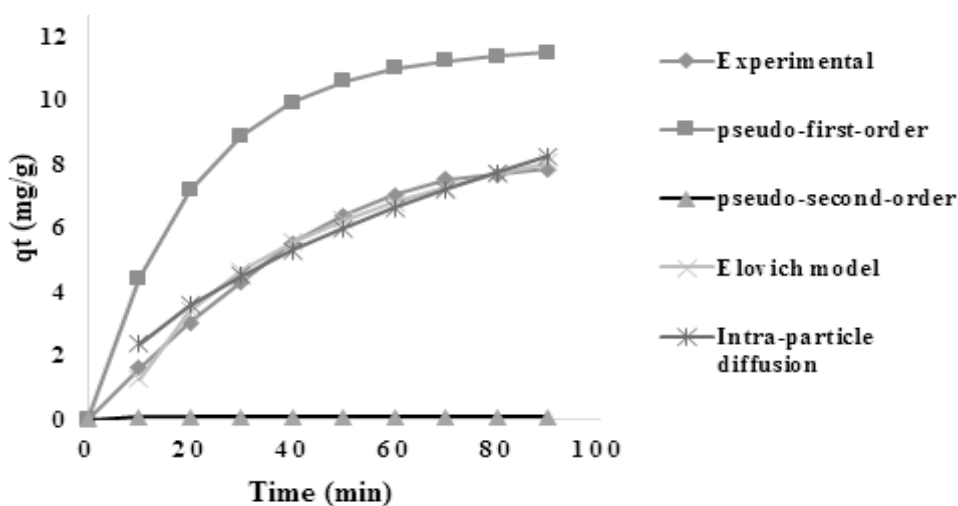


**Fig. 10.** Nonlinear adsorption rate curves (q<sub>t</sub> vs t) (Cd concentration: 40 ppm; cat.: 0.05g; pH: 6.5; r.t.)

The nonlinear plots of adsorption kinetic are shown in Figure 10. The plot related to Elovich equation is more fitted with the plot of experimental data.

### 3.4. Thermodynamic study

The thermodynamic behavior of Cd adsorption was investigated by the calculation of thermodynamic parameters using the following equations [24]:

$$\Delta G^\circ = -RT \ln K_c$$

$$\ln K_c = \frac{T \Delta S^\circ - \Delta H^\circ}{RT}$$

$$K_c = \frac{q_e}{C_e}$$

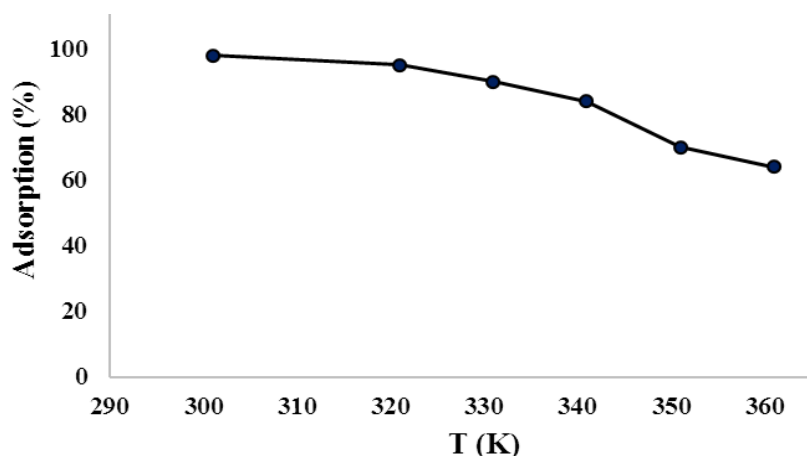
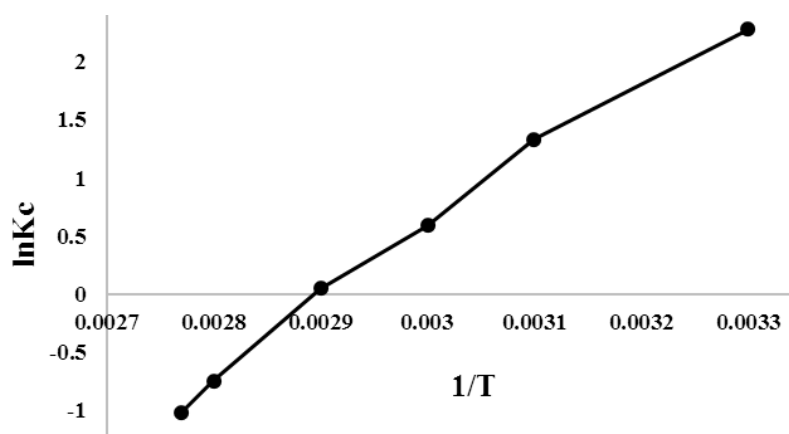
K<sub>c</sub> (L/mg) is the equilibrium constant,  
R = 8.314 J/mol·K  
T is the absolute temperature (K)  
Gibbs free energy ΔG°(kJ/mol)  
Enthalpy ΔH°(kJ/mol)  
Entropy ΔS° (J/K·mol)

Figure 11 shows the adsorption efficiency of NiO-SnO<sub>2</sub> nano-composite at different temperatures (28-

78°C). As can be seen from Figure 11, increasing temperature has an adverse effect on the adsorption capacity as the adsorption percent is decreasing with heat increasing. The linear plots of lnK<sub>c</sub> vs 1/T and above equations (Figure 12) were used for the calculation of thermodynamic parameters. The results are summarized in Table 3. The values of ΔS° and ΔH° are negative while ΔG° is positive. The exothermic nature of Cd adsorption as confirmed by negative amount of ΔH° causes it to reduce the absorption rate by increasing the temperature. The non-spontaneous nature of Cd adsorption is shown by positive values of ΔG°. While the randomness of the Cd adsorption demonstrated by the negative values of ΔS° [24].

**Table 3.** Thermodynamic parameters of Cd adsorption

$\Delta S^\circ$ (j/mol)	$\Delta H^\circ$ (Kj/mol)	T(K)	$K_c$	$\Delta G^\circ$ (Kj/mol)
-151.3148	-6.25	301	9.8	+ 39.25
		321	3.8	+42.32
		331	1.8	+43.83
		341	1.05	+45.35
		351	0.47	+46.86
		361	0.36	+48.37

**Fig. 11.** Adsorption of Cd: effect of temperature (time: 90min; cat.: 0.05g; Cd concentration: 40 ppm; pH: 6.5; r.t.)**Fig. 12.** linear plot of  $\ln K_c$  vs  $1/T$ 

#### 4. Conclusions

In summary, NiO – SnO<sub>2</sub> nano-composites were successfully prepared *via* co-precipitation reaction of NiCl<sub>2</sub> and SnCl<sub>2</sub> in a grape extract media and characterized by XRD, FE-SEM, DLS, and BET techniques. The capacity of the nano-composites for the removal of cadmium ions from aqueous media was investigated. In comparison nanocomposites that prepared in grape extract media show higher surface area and removal capacity for Cd ions.

#### Acknowledgments

We are thankful to the Lahijan Branch, Islamic Azad University research council for partial support of this research

#### References

[1] Dehbashi, M.; Aliahmad, M.; Shafiee, M. R. M.; Ghashang, M. SnO<sub>2</sub> Nanoparticles: Preparation and

Evaluation of Their Catalytic Activity in the Oxidation of Aldehyde Derivatives to Their Carboxylic Acids and Sulfides to Sulfoxide Analogues. *Phosphorus Sulfur Silicon Relat. Elem.* 2013, 188, 864–872.

[2] Dehbashi, M.; Aliahmad, M.; Shafiee, M. R. M.; Ghashang, M. Nickel-Doped SnO<sub>2</sub> Nanoparticles: Preparation and Evaluation of Their Catalytic Activity in the Synthesis of 1-Amidoalkyl-2-naphthols. *Inorg. Nano-Met. Chem.* 2013, 43, 1301–1306.

[3] Dehbashi, M.; Aliahmad, M.; Shafiee, M. R. M.; Ghashang, M. NiO–SnO<sub>2</sub> Composite Nanopowder: Preparation and Evaluation of Their Catalytic Activity in the Synthesis of 1-Amidoalkyl-2-naphthols. *Lett. Org. Chem.* 2012, 9, 711–719.

[4] D'Arienzo, M.; Cristofori, D.; Scotti, R.; Morazzoni, F. New Insights into the SnO<sub>2</sub> Sensing

- Mechanism Based on the Properties of Shape-Controlled Tin Oxide Nanoparticles. *Chem. Mater.* 2013, 25, 3675–3686.
- [5] Desarkar, H. S.; Kumbhakar, P.; Mitra, A. K. Optical Properties of Tin Oxide Nanoparticles Prepared by Laser Ablation in Water: Influence of Laser Ablation Time and Laser Fluence. *Mater. Charact.* 2012, 73, 158–165.
- [6] Bhattacharjee, A.; Ahmaruzzaman, M. Photocatalytic Degradation and Reduction of Organic Compounds Using SnO<sub>2</sub> Quantum Dots via a Green Route under Direct Sunlight. *RSC Adv.* 2015, 5, 66122–66123.
- [7] Pianaro, S. A.; Bueno, P. R.; Olivi, P.; Longo, E.; Varela, J. A. Electrical Properties of SnO<sub>2</sub>-Based Varistors. *J. Mater. Sci.: Mater. Electron.* 1998, 9, 159–165.
- [8] Fortunato, E.; Ginley, D.; Hosono, H.; Paine, D. C. Transparent Conducting Oxides for Photovoltaics. *MRS Bull.* 2007, 32, 242–247.
- [9] Park, S. H.; Son, Y. C.; Willis, W. S.; Suib, S. L.; Creasy, K. E. Tin Oxide Films Prepared by Physical Vapor Deposition–Thermal Oxidation and Spray Pyrolysis. *Chem. Mater.* 1998, 10, 2389–2398.
- [10] Ateş, S.; Baran, E.; Yazici, B. Fabrication of Al<sub>2</sub>O<sub>3</sub> Nanopores/SnO<sub>2</sub> and Its Application in Photocatalytic Degradation under UV Irradiation. *Mater. Chem. Phys.* 2018, 214, 17–27.
- [11] Liu, B.; Gao, L.; Zhou, F.; Duan, G. Preferential Epitaxial Growth of β-FeOOH Nanoflakes on SnO<sub>2</sub> Hollow Spheres for the Synthesis of SnO<sub>2</sub>/α-Fe<sub>2</sub>O<sub>3</sub> Heteronanocomposites with Enhanced Gas Sensing toward Dimethyl Disulfide. *Sens. Actuators, B* 2018, 272, 348–360.
- [12] Shaposhnik, D.; Pavelko, R.; Llobet, E.; Gispert-Guirado, F.; Vilanova, X. Hydrogen Sensors Based on SnO<sub>2</sub>–TiO<sub>2</sub> Systems. *Procedia Eng.* 2011, 25, 1133–1136.
- [13] Kumar, S.; Nigam, R.; Kundu, V.; Jaggi, N. Sol–Gel Synthesis of ZnO–SnO<sub>2</sub> Nanocomposites and Their Morphological, Structural, and Optical Properties. *J. Mater. Sci.: Mater. Electron.* 2015, 26, 3268–3274.
- [14] Zhang, J.; Zeng, D.; Zhu, Q.; Wu, J.; Huang, Q.; Zhang, W.; Xie, C. Enhanced Room-Temperature NO<sub>2</sub> Response of NiO–SnO<sub>2</sub> Nanocomposites Induced by Interfacial Bonds at the p–n Heterojunction. *Phys. Chem. Chem. Phys.* 2016, 18, 5386–5396.
- [15] Ghashang, M.; Mansoor, S. S.; Mohammad Shafiee, M. R.; Kargar, M.; Najafi Biregan, M.; Azimi, F.; Taghrir, H. Green Synthesis of MgO Nanopowders as Efficient Catalysts for Thiochromeno[4,3-b]pyran and Thiopyrano[4,3-b]pyran Derivatives. *J. Sulfur Chem.* 2016, 37, 377–390.
- [16] Ghashang, M.; Mansoor, S. S.; Shams Solaree, L.; Sharifian-Esfahani, A. One-Pot Multicomponent Aqueous Synthesis of Dihydropyrano[3,2-c]chromene Derivatives over MgO Nanoplates. *Iran. J. Catal.* 2016, 6, 237–243.
- [17] Ghashang, M.; Kargar, M.; Shafiee, M. R. M.; Mansoor, S. S.; Fazlinia, A.; Esfandiari, H. CuO Nanostructures Prepared in Rosmarinus officinalis Leaf Extract Medium as Efficient Catalysts for the Aqueous Synthesis of Dihydropyrano[3,2-c]chromene Derivatives. *Recent Pat. Nanotechnol.* 2015, 9, 204–211.
- [18] Mobinikhaledi, A.; Yazdanipour, A.; Ghashang, M. Green Synthesis of MgO Grit-Like Nanostructures as Efficient Catalysts for 4H-Pyrans and α,α'-Bis(substituted benzylidene) cycloalkanones. *Green Process. Synth.* 2016, 5, 289–295.
- [19] Shafiee, M. R. M.; Kargar, M.; Ghashang, M. Characterization and Green Synthesis of Zn<sup>2+</sup>-Doped MgO Nanoparticles. *Green Process. Synth.* 2018, 7, 248–254.
- [20] Shafiee, M. M. R.; Kargar, M.; Hashemi, M. S.; Ghashang, M. Green Synthesis of NiFe<sub>2</sub>O<sub>4</sub>/Fe<sub>2</sub>O<sub>3</sub>/CeO<sub>2</sub> Nanocomposite in Walnut Green Hull Extract: Magnetic Properties and Characterization. *Curr. Nanosci.* 2016, 12, 645–649.
- [21] Bahrudin, N. N.; Nawi, M.; Lelifajri, A. Kinetics and Isotherm Modeling of Phenol Adsorption onto Immobilized Activated Carbon. *React. Kinet. Mech. Catal.* 2019, 126, 61–82.
- [22] Aminsharei, F.; Lahijanian, A.; Shiehbeigi, A.; Shieh Beiki, S.; Ghashang, M. Dual Magnetization and Amination of Cellulosic Chains for the Efficient Adsorption of Heavy Metals. *Int. J. Biol. Macromol.* 2024, 276, 134004. <https://doi.org/10.1016/j.ijbiomac.2024.134004>.
- [23] Rajaei, A. N.; Mohammadi, F.; Ghashang, M. NiFe<sub>2</sub>O<sub>4</sub>@SiO<sub>2</sub>-NH-Cellulose-Protein Composite Biopolymer as a Modified Cysteine-Rich Protein Structure for Heavy Metals Removal from Wastewater. *Int. J. Biol. Macromol.* 2025, 314, 144404. <https://doi.org/10.1016/j.ijbiomac.2025.144404>.
- [24] Sheikh, S.; Naghizadeh-Dehno, O.; Mirkhalafi, S.; Ghashang, M. Magnetic Heterogenization of Supramolecular Carbohydrates for the Efficient Adsorption of Heavy Metals Removal from Wastewater. *Inorg. Chem. Commun.* 2024, 168, 112835. <https://doi.org/10.1016/j.inoche.2024.112835>